JACS
JOURNAL OF THE AMERICAN CHEMICAL SOCIETY
pubs.acs.org/JACS
Article

Evidence for Many Unique Solution Structures for Chymotrypsin Inhibitor 2: A Thermodynamic Perspective Derived from vT-ESI-IMS-MS Measurements

Shannon A. Raab, Tarick J. El-Baba, Daniel W. Woodall, Wen Liu, Yang Liu, Zane Baird, David A. Hales, Arthur Laganowsky, David H. Russell, and David E. Clemmer*

Cite This: J. Am. Chem. Soc. 2020, 142, 17372−17383

ABSTRACT: Chymotrypsin inhibitor 2 (CI-2) is a classic model for two-state cooperative protein folding and is one of the most extensively studied systems. Alan Fersht, a pioneer in the field of structural biology, has studied the wild-type (wt) and over 100 mutant forms of CI-2 with traditional analytical and biochemical techniques. Here, we examine wt CI-2 and three mutant forms (A16G, K11A, L32A) to demonstrate the utility of variable-temperature (vT) electrospray ionization (ESI) paired with ion mobility spectrometry (IMS) and mass spectrometry (MS) to map the free energy folding landscape. As the solution temperature is increased, the abundance of each of the six ESI charge states for wt CI-2 and each mutant is found to vary independently. These results require that at least six unique types of CI-2 solution conformers are present. Ion mobility analysis reveals that within each charge state there are additional conformers having distinct solution temperature profiles. A model of the data at ∼30 different temperatures for all four systems suggests the presence of 41 unique CI-2 solution conformations. A thermodynamic analysis of this system yields values of ΔC_p as well as ΔG, ΔH, and ΔS for each state at every temperature studied. Detailed energy landscapes derived from these data provide a rare glimpse into Anfinsen's thermodynamic hypothesis and the process of thermal denaturation, normally thought of as a cooperative two-state transition involving the native state and unstructured denatured species. Specifically, as the temperature is varied, the entropies and enthalpies of different conformers undergo dramatic changes in magnitude and relative order to maintain the delicate balance associated with equilibrium.

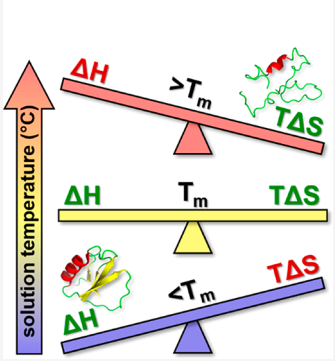

INTRODUCTION

In their classic 1963 paper, "The Genetic Control of Tertiary Protein Structure: Studies With Model Systems",[1] Epstein, Goldberger, and Anfinsen argued that "According to [the thermodynamic] hypothesis, the particular configuration that a protein assumes, under any specific set of conditions, is the one that is thermodynamically the most stable." Implicit in this statement is the idea that many different structures would be favored as one changes conditions that influence a protein's stability (e.g., environmental factors such as temperature,[2,3] solvent,[4,5] and pH,[6] as well as post-translational modifications,[7−9] interactions with ligands,[10,11] and formation of protein complexes). Computations support this.[12−14] Unlike the simple solid-to-liquid phase transitions that occur upon destabilizing small-molecule crystals, denaturation of proteins involves distributions of structures.[15−18] But, rarely is it possible to experimentally observe these higher-energy, low-abundance species,[19,20] even near the transition region for denaturation. Structural changes of polypeptide chains are observed as cooperative, two-state processes that occur when well-ordered, functional (native) structures become unstable—unfolding to produce distributions of non-native (denatured) states.[21] And, very little is known about these non-native species.

In the work presented below, we use a variable-temperature (vT) electrospray ionization (ESI) source coupled with ion mobility spectrometry (IMS) and mass spectrometry (MS) techniques to investigate the thermal denaturation of a 64-residue truncated form of chymotrypsin inhibitor 2 (CI-2), a well-characterized, textbook model system that was developed by Fersht and his collaborators.[21,22] In addition to wild-type (wt) CI-2, detailed studies were carried out on three mutants: a sequence in which a Gly residue is substituted for Ala[16] (A16G), one having Ala substituted for Lys[11] (K11A), and a mutant having Ala substituted for Leu[32] (L32A). These data and analyses are provided in the Supporting Information (SI). The evaporative cooling phenomenon associated with ESI droplet shrinkage and ion formation "freezes out" populations of solution species, and in the absence of lubricating solvent, different antecedent states are trapped as ions, each with

Received: May 15, 2020
Published: August 31, 2020

https://dx.doi.org/10.1021/jacs.0c05365
J. Am. Chem. Soc. 2020, 142, 17372−17383

distinct shape and charge, which can be investigated during their short residence times in the spectrometer.[23,23,24]

The truncated 64-residue form of CI-2 (Scheme 1) was chosen for these vT-ESI-IMS-MS studies because the transition between folded and denatured states is thoroughly characterized.[21] Crystallographic[25] and solution nuclear magnetic resonance[26] studies show that under native conditions CI-2 adopts an α/β configuration such that a mixed parallel and anti-parallel β-sheet packs against a single α-helix to form the hydrophobic core.[22] Differential scanning calorimetry (DSC) and chemical denaturation measurements are consistent with a simple process involving only two states.[21] Detailed studies of more than 100 mutant forms reveal a weakly formed transition state, suggesting a nucleation–condensation mechanism of folding where a structured nucleus consolidates favorable long-range interactions to form the native structure.[27,28]

Scheme 1. Amino Acid Sequence (Top) and Cartoon Representation (Bottom) of Truncated wt CI-2 (PDB: 2CI2), with Sites Chosen for Mutation in Bold

1-20	LKTEWPELVG **K**SVEE**A**KKVI
21-40	LQDKPEAQII V**L**PVGTIVTM
41-60	EYRIDRVRLF VDKLDNIAEV
61-64	PRVG

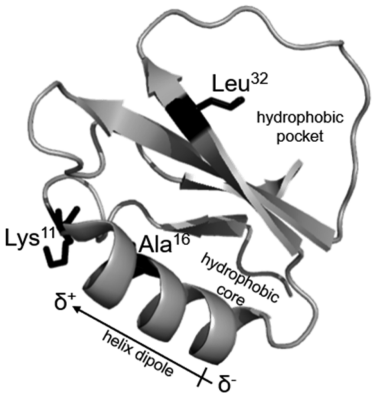

Because the truncated form of CI-2 is relatively small, it is attractive for IMS-MS studies. Unlike larger proteins, small peptides often show sharp, mobility-resolved peaks associated with isolation of specific conformations.[29−35] Mobility measurements for larger proteins typically yield broad peaks,[36−38] indicating that many structures have similar cross sections and thus are not resolved.[39,40] We suspected that the 64-residue truncated CI-2 might allow similar conformer types to be resolved, making it possible to discern many closely related precursor and product species. As shown below, this is the case. We find evidence for many discrete solution structures. An analysis and model of these data provide evidence that 41 structural transitions are involved in the thermal denaturation of CI-2. From changes in the abundances of these species with solution temperature, we extract detailed thermochemistry (ΔG, ΔH, ΔS, and ΔC_p) for each state at 30 solution temperatures (from 22 to 80 °C) over the range of the melting transition. Many of the observed species exist in only minute abundances. Because of the exceptional sensitivity and dynamic range of IMS-MS techniques, it is straightforward to quantify complex many-state solution equilibria where unique conformers differ in abundances by over 4, or, in some cases, even 5 orders of magnitude—far beyond the dynamic range and detection limits of traditional calorimetric methods. The ability to quantify species over such a wide range allows us to determine a free energy landscape that includes species that are much less stable than have ever been reported experimentally. By definition, near each conformer's melting temperature (T_m), its enthalpy and entropy are balanced (i.e., $\Delta H \approx T\Delta S$). In this paper, we show that above and below the T_m of each, this balance is harder to maintain, and slight offsets control the populations of native and denatured states.

While these data provide a remarkable glimpse into the intricate balance of populations of many species that appear and disappear as a protein undergoes thermal denaturation, we note that the issue of structural characterization of non-native states remains elusive. But, the present data provide some clues and opportunities for future studies. Collision cross sections are a measure of the sizes of ions in the gas phase, and to the extent that these can be computationally described and then translated into solvated conformers, they provide a structural constraint.[4,38,41−45] Thermodynamic values provide additional constraints that should be testable by theory. In addition to insight about stability (from values of ΔH) and conformer accessibility (from ΔS), values of ΔC_p can be associated with differences in the solvent exposure of more or less polar side chains,[46] offering an additional constraint for characterizing structures and structural changes.

EXPERIMENTAL SECTION

vT-ESI-IMS-MS Measurements. Experiments were carried out using a home-built 4-m long drift tube/time-of-flight (TOF) mass spectrometer (Figure S1) which records nested IMS-MS data.[47−49] A detailed description of IMS-MS instrumentation is found elsewhere.[50−53] Briefly, ions generated by ESI enter the IMS-MS instrument source through a narrow capillary and are stored in an hourglass ion funnel[54,55] until they are pulsed into a 4-m drift tube by lowering an electrostatic gate for 100 μs. Protein ions traverse the drift tube filled with a buffer gas (~2.5 Torr He) under the influence of a weak electric field (~12 V·cm^{-1}). Protein structures are separated based on size, shape, and charge.[38] Drift times are converted to cross sections as described in the SI. Ions exit the drift region and are pulsed into an orthogonal two-stage reflectron geometry TOF mass analyzer and are detected by microchannel plates. To induce thermal denaturation, a custom-built temperature-controlled ESI source similar to those described by our group[3] and others[56−58] was used (Figure S2).

Determination of Ensemble Melting Temperatures from Analysis of Weighted Average of Charge State Distributions Recorded at Varying Solution Temperatures. Benesch and co-workers have reported a simple means of determining melting temperatures based on the changes in the ESI protein charge state distribution as a function of solution temperature.[59] Here, the intensities of different charge states are used to compute the weighted average charge state ($\bar{z}$) determined at each solution temperature, as described by eq 1:

$$\bar{z} = \frac{\sum_j^n z_j i_j}{\sum_j^n i_j} \quad (1)$$

where i_j is the intensity of a mass spectrum peak having a charge state of z_j. Melting/formation temperatures (T_m/T_f) are determined as the midpoint of the transition according to a fit with a sigmoidal function as described previously[3] using the nonlinear curve fit tool and the Boltzmann function in OriginPro shown in eq 2:

https://dx.doi.org/10.1021/jacs.0c05365
J. Am. Chem. Soc. 2020, 142, 17372−17383

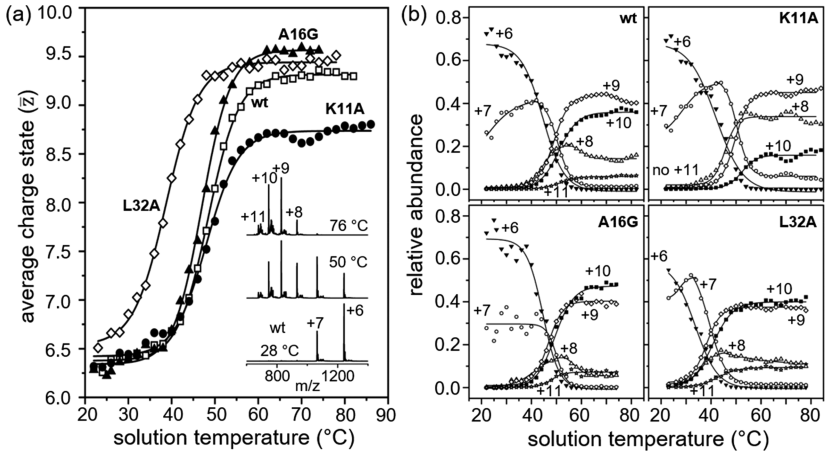

Figure 1. (a) Average charge state as a function of solution temperature with two-state fit for wt CI-2 (□) with T_m = 48.4 ± 0.1 °C, K11A (●) with T_m = 48.0 ± 0.2 °C, A16G (▲) with T_m = 47.0 ± 0.2 °C, and L32A (◇) with T_m = 38.7 ± 0.2 °C; inset shows mass spectra at solution temperatures 28, 50, and 76 °C for wt CI-2. (b) Relative abundance as a function of solution temperature for each observable charge state for all sequence variants.

$$y(T) = y_{max} + \frac{y_{min} - y_{max}}{1 + \exp\frac{(T - T_m)}{dT}} \quad (2)$$

where y_{max} and y_{min} are the maximum and minimum y-values. All data were processed using OriginPro 2018 software (OriginLab Corp., Northampton, MA, USA).

Modeling of Cross Section Distributions to Obtain Insight about the Numbers and Abundances of Solution Structures. Within each MS charge state, IMS distributions show that additional conformations are present. The abundances of features within these distributions vary with temperature but are often only partially resolved. In order to make use of this information, we have modeled these data with a set of Gaussian functions. In this analysis, we require that a single set of defined Gaussian functions be capable of representing all temperatures for each of the four sequences. That is, we hold the position and width of each distribution constant and vary only its intensity. We interpret each Gaussian distribution as a representation of a conformation type from solution, denoted by charge state and number (e.g., the fourth fitted Gaussian function in the +6 charge state is denoted conformer 6.4). Once the model features are determined, an automated iterative algorithm is used to determine the best fit and solution conformer abundances. In some cases, the abundance profiles of several Gaussian distributions have nearly identical temperature dependences. We assume that these features observed in the gas-phase data emerge from a single conformation type in solution. Thus, we combine the populations of these features and treat them as a single conformer family. It is important to stress that the model ultimately captures the main features associated with ∼120 independent datasets (i.e., ∼30 temperatures for each of the four CI-2 sequences). While we have attempted to automate this process (see SI), our best model comes from a manual iterative analysis. A complete discussion of this analysis is provided in the SI. Because the intensities are inherently model dependent, we note that other models with fewer or more components may also represent these data. As long as the numbers of total features for the reference state and other states change proportionally, the relative thermochemistry will remain similar.

Thermodynamic Analysis by the Gibbs–Helmholtz Relationship. The Gibbs–Helmholtz[60] equation is used to obtain thermodynamic values for CI-2. For this analysis, the abundance of each conformer family at each solution temperature is converted to a free energy value, ΔG. The equilibrium constant $K_j(T)$ for each conformer family is calculated from the relative abundance of a conformer family at a specific solution temperature $[I_j(T)]$ with reference to the relative abundance of the reference state, product group 1 (see SI), at the same solution temperature $[P_1(T)]$, as shown by eq 3:

$$K_j(T) = \frac{I_j(T)}{I_{P_1}(T)} \quad (3)$$

The value for $\Delta G(T)$ is then calculated for each conformer group using eq 4:

$$\Delta G(T) = -RT \ln(K_{eq}(T)) \quad (4)$$

where R is the gas constant, T is the solution temperature, and $K_{eq}(T)$ is the equilibrium constant for a conformer group as calculated using eq 3. Plots of ΔG versus solution temperature are generated for each conformer family, and a nonlinear least-squares optimization is used to fit each $\Delta G(T)$ plot to solve for values of enthalpy (ΔH), entropy (ΔS), and heat capacity (ΔC_p) using the Gibbs–Helmholtz equation:

$$\Delta G(T) = \Delta H_R - T\Delta S_R + \Delta C_p\left[T - T_R - T \ln\left(\frac{T}{T_R}\right)\right] \quad (5)$$

where ΔH_R is the enthalpy at the reference temperature T_R (arbitrarily set at 323.15 K) and ΔS_R is the entropy at T_R.

RESULTS AND DISCUSSION

Analysis of Average ESI Charge State as a Function of Solution Temperature. The inset in Figure 1a shows representative mass spectra acquired for an aqueous solution of wt CI-2 (pH ≈ 2.6) at solution temperatures 28, 50, and 76 °C. At 28 °C, the wt mass spectrum is dominated by the $[M + 6H]^{6+}$ species at m/z 1242 and the +7 charge state at m/z 1065. This narrow distribution comprised of low-charge species is consistent with a compact structure having six to seven surface-exposed basic residues protonated. At 50 °C, the +6 charge state has markedly decreased in abundance and the MS distribution shifts to favor several signals at lower m/z assigned as the +8 through +11 charge states. At 76 °C, a distribution centered around the +9 and +10 charge states emerges. This trend is observed for the mutant sequences as well, shown in Figure S3; however, K11A does not accommodate 11 charges at high temperatures, suggesting K^{11} is a prominent site for protonation for the unfolded structures of CI-2.

A shift in charge state with temperature signifies a structural change—as the protein elongates, basic core residues become exposed to the aqueous solvent and are protonated.[2,32,61] For a discussion on the influence of solution conformation on ESI

https://dx.doi.org/10.1021/jacs.0c05365
J. Am. Chem. Soc. 2020, 142, 17372–17383

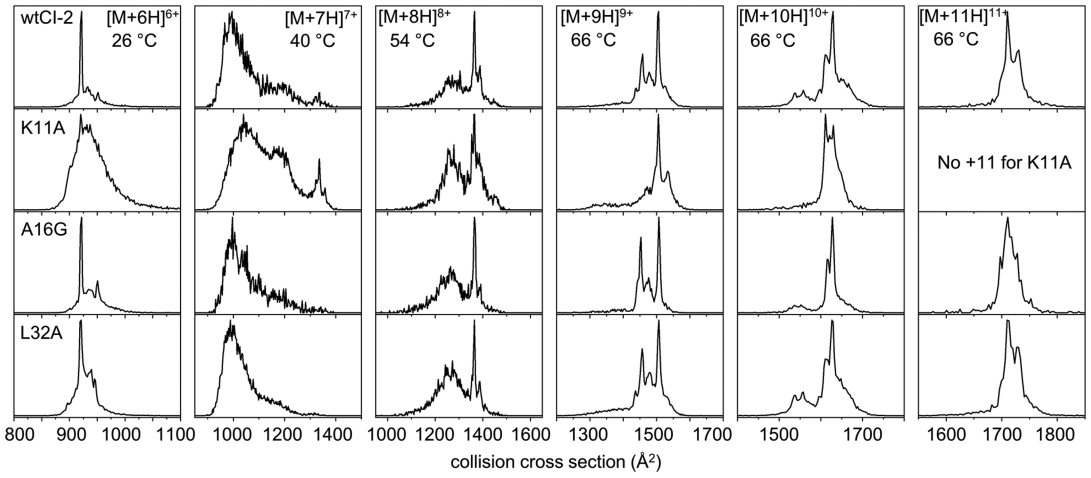

Figure 2. Mobility distributions at representative solution temperatures for the +6 through +11 charge states for each CI-2 sequence (wt, K11A, A16G, and L32A).

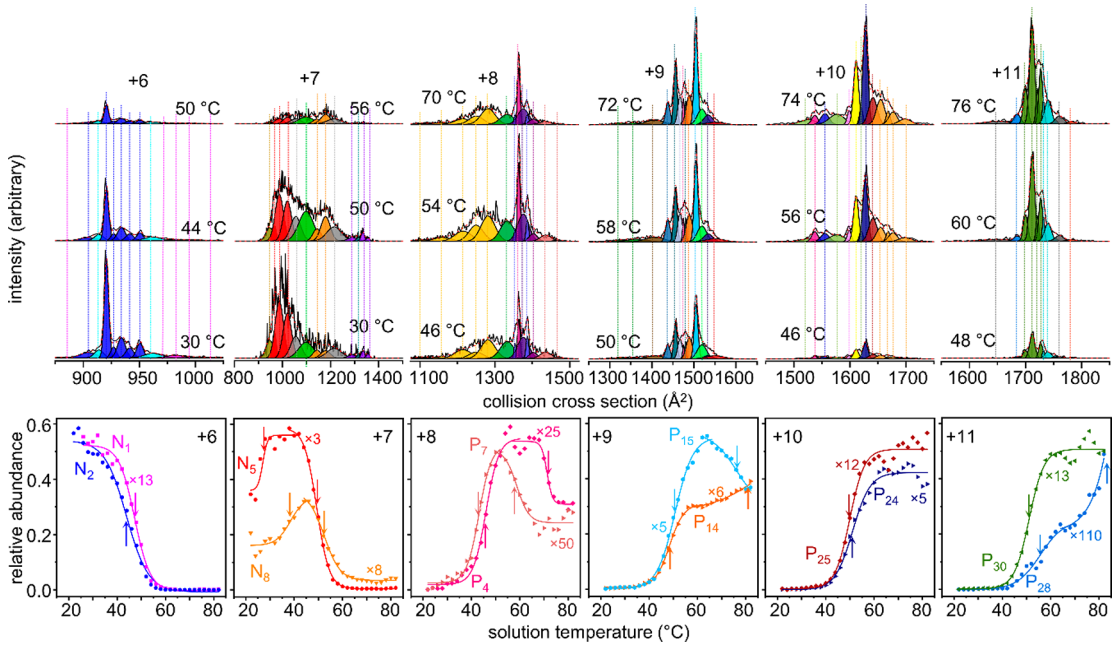

Figure 3. Top panel shows modeled collision cross section distributions of wt +6 through +11 charge states at representative low, medium, and high solution temperatures. Vertical lines represent peak centers for each Gaussian function, and the color represents the corresponding conformational group determined from grouping analysis of the wt and mutant data. The bottom panel shows scaled plots of the relative abundance of representative groups as a function of solution temperature. The arrows indicate the respective T_m or T_f values for each conformer family.

charge states, see the SI. A quantitative view of this is obtained by plotting the weighted average charge state as a function of solution temperature[59] as shown in Figure 1a for the wt and each mutant. The T_m for each sequence is obtained by fitting these data to a two-state transition as described by eq 2. T_m values provide an overall signature for stability such that a protein with a high T_m is more stable than a protein with a lower T_m. Analysis of the wt data yields T_m = 48.4 ± 0.1 °C, in agreement with T_m values at similar pH reported from DSC analysis.[21] See the Figure 1 caption for mutant T_m values, and Table S1 for a comparison of mutant $\Delta\Delta G$ values obtained from IMS-MS measurements and traditional methods.[21,27,28]

Evidence for Differences in Conformation Types from the Temperature Dependence of Individual Charge States. The MS data are further analyzed by plotting the relative abundances of the individual charge states as a function of solution temperature as shown in Figure 1b. In the wt plot, the +6 charge state decays with increasing temperature at T_m = 44.5 ± 0.4 °C, a value significantly lower than the overall T_m obtained from the wt average charge analysis. Between 20 and 45 °C, the wt +7 increases in abundance before decaying at T_m = 50.5 ± 0.1 °C. The +8 through +11 charge states increase distinctively with further increases in solution temperature, as shown in Figure 1b and Table S2. That the abundance of each of the six ESI charge states changes uniquely with solution temperature (i.e., T_m and T_f values, curve shapes) provides evidence for a minimum of six distinct conformation types. Often, the abundances of protein charge states appear as a statistical distribution, suggesting a single (or at most a few) antecedent solution conformation(s).[62−64]

The charge state behavior of the mutants with increasing solution temperature is also shown in Figure 1b and described

https://dx.doi.org/10.1021/jacs.0c05365
J. Am. Chem. Soc. 2020, 142, 17372−17383

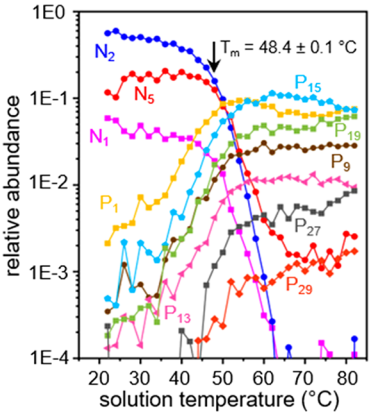

Conformer	Structures grouped	T_{f1} (°C)[a]	T_{m1} (°C)[b]	T_{f2} (°C)[c]
N_1 (■)	6.1, 6.10–6.14		47.2 ± 0.2	
N_2 (●)	6.2, 6.4–6.8		43.9 ± 0.4	
N_5 (●)	7.2–7.4	27.0 ± 0.3	49.4 ± 0.1	
P_1 (□)	8.1–8.5	45.2 ± 0.2	61.0 ± 0.4	77.5 ± 0.1
P_9 (●)	9.3	49.1 ± 0.2		
P_{13} (◁)	9.7	49.5 ± 0.3		
P_{15} (⬠)	9.10	50.7 ± 0.2	76.3 ± 2.8	
P_{19} (■)	10.1, 10.4, 10.7	50.2 ± 0.2		75.5 ± 0.5
P_{27} (■)	11.1, 11.10	51.8 ± 0.3		78.3 ± 0.5
P_{29} (◆)	11.11	61.5 ± 3.0		

[a-c]midpoint melting (T_m) or formation (T_f) temperature as determined from sigmoidal fit of peak areas as a function of temperature; error values are reported from the fit

Figure 4. Relative abundance as a function of solution temperature plot for ten out of the 41 precursor or product groups (left) and their corresponding grouping analysis and T_f or T_m values shown in the table (right).

in Table S2. The T_m and T_f for each transition have unique values, and the abundances of the charge states for each mutant vary. Therefore, while global structural transitions of the wt and mutant sequences appear similar, each sequence stabilizes a unique distribution of conformer types at each solution temperature during thermal denaturation.

Overview of Mobility Distributions for wt, K11A, A16G, and L32A CI-2. IMS distributions provide a unique opportunity to examine the effects of a single amino acid mutation on the structures of CI-2. Figure 2 shows mobility distributions for the observed charge states +6 through +11 at representative solution temperatures for wt CI-2 and the mutant data corrected with intrinsic size parameters.[65] The +6 mobility distribution for wt at 26 °C shows a sharp feature centered around 920 Å^2 and a small population of features from ~920 to 970 Å^2. This distribution is not significantly altered by the A16G and L32A mutations; however, the K11A +6 mobility distribution depicts increased abundance of the elongated mobility features, a result that has been reproduced multiple times.

The +7 mobility distributions span from 900 and 1400 Å^2, which is significantly broader than the mobility distribution for the +6 charge state, implying that a large range of structures present as +7 ions. The +7 distribution includes a compact feature centered about 1000 Å^2, a population around 1175 Å^2, and a small distribution of elongated structures around 1350 Å^2. The +7 distributions also appear very similar between mutant variants, but the populations of structures vary. Inspection of the high charge states +8 through +11 for each sequence offers examples of structures that are unfavored once a mutation is made. For instance, the +9 distribution for wt shows two main features at 1440 and 1520 Å^2. The feature centered around 1520 Å^2 is conserved throughout each sequence, but the feature at 1440 Å^2 is almost completely absent in the K11A dataset.

Determining the Minimum Number of Solution States at Different Temperatures. Because there are numerous features in the mobility distributions, it is useful to model the IMS data with a set of Gaussian functions, as described above and in the SI. This analysis requires that the same set of Gaussian functions is used to describe the temperature- and sequence-variant IMS distributions. The mobility distributions for each charge state require between 11 and 14 Gaussian functions to reach a proper fit (R^2 > 0.90), and a total of 77 Gaussian functions were required to model all mobility distributions (Table S3). The modeled IMS distributions for the wt sequence are shown at the top of Figure 3 and the mutant models are found in Figures S9–S14.

The normalized area of each Gaussian function is plotted against solution temperature to obtain relative abundance profiles. Conformers that show similar thermal behavior (i.e., similar T_m or T_f values, cross sections, and solution temperature profiles) are grouped and treated as a single conformational family. This analysis helps to avoid overestimation of the number of unique CI-2 conformations. In some cases, this approach may cause us to combine some unique solution states that have the same thermal properties. As an example, the +6 distribution shows several features having indistinguishable temperature profiles but different cross sections. The relative abundance plots for the wt sequence of all 77 modeled Gaussian functions and their grouping analysis are shown in Figures S15 and S16. When we consider the grouping analysis of all 77 modeled Gaussian functions for just the wt sequence, we find five precursor structures (denoted N_1–N_5) that decay at unique temperatures to form 12 product structures (P_1–P_{12}) at varying temperatures as summarized in Figure S17.

The mutant data provide an additional means of determining the smallest number of unique conformations that must comprise the thermal denaturation of wt CI-2. First, the mutant IMS datasets are grouped into the same conformational families as determined from the wt analysis described above. The presence of a unique mutant conformer implies that the corresponding conformer in the wt data is unique also; i.e., the structure that exhibits unique thermal behavior upon mutation is affected differently by the change in sequence compared to the other structures within the same wt family. In this case, mutant structures that do not fit within the wt grouping are ungrouped to create a new wt conformational family. A detailed description of this analysis is provided in the SI, and the grouping analysis using the mutant datasets in this way is shown in Figures S18–S20.

From analysis of both the wt and mutant datasets, we find evidence for 41 unique structures (Table S4, Figure S21). Ten precursor states (N_1–N_{10}), which presumably correspond to structures that reflect the distribution of "native" structures, elongate to form 31 unique product conformations (P_1–P_{31}). Examples of relative abundance plots for some conformational families are shown at the bottom of Figure 3. The abundance profiles for conformer families N_1 (magenta) and N_2 (blue) in

https://dx.doi.org/10.1021/jacs.0c05365
J. Am. Chem. Soc. 2020, 142, 17372–17383

the +6 charge state have different T_m values at 47.2 ± 0.2 °C and T_m = 43.9 ± 0.4 °C, respectively. In this case, N_1 represents structures that are more stable than structures grouped in N_2. Analysis of the +8 and +9 conformer families show relative abundance plots that increase with temperature and subsequently decay at higher temperatures. This implies that structures that present as +8 and +9 ions are less abundant at higher temperatures where structures in the +10 and +11 charge states dominate.

The relative abundances of 10 representative conformers (N_1, N_2, N_5, P_1, P_9, P_{13}, P_{15}, P_{19}, P_{27}, and P_{29}) resulting from the grouping analysis are shown in Figure 4 as a function of solution temperature across 4 orders of magnitude. The incredible sensitivity and dynamic range of vT-ESI-IMS-MS allows us to sample low-abundance structures that are often beyond the limit of detection for traditional techniques. This method has allowed us to provide evidence for 41 unique structures of wt CI-2 that each undergo unique two-state transitions with increasing solution temperature.

Thermodynamic Analysis: Examples of ΔG at Solution Temperatures of 26, 46, and 74 °C for Each of the 41 Unique Solution Conformers of wt CI-2. An explanation of our choice of a reference point for the thermodynamic analysis is provided in the SI. Values of ΔG for all 41 wt CI-2 conformer types with respect to conformer P_1 are derived at all solution temperatures, see Tables S5−S8. Figure 5 shows examples for three solution temperatures (26, 46, and 74 °C). It is interesting to plot values of ΔG against the measured cross sections for each conformer (within each charge state) as these plots resemble free energy landscapes. These landscapes provide a rare experimental opportunity to determine the relative energetics of many conformers; as shown below, the changes that are observed with increasing temperature offer insight about the driving forces involved in thermal denaturation.

At 26 °C (Figure 5a), precursors, observed as the abundant populations of the cross section distributions for the +6 and +7 charge states, have favorable free energies ranging from ca. −12 to 2 kJ·mol^{-1}. Products of melting, the scarcely populated species observed experimentally as the cross section distributions for the +8 through +11 charge states, have less favorable free energies (i.e., ca. 0 to 20 kJ·mol^{-1}). The large range (~32 kJ·mol^{-1}) of free energies (from ca. −12 to 20 kJ·mol^{-1}) favor the more compact ions observed for the +6 and +7 charge states (ca. 700 to 1340 Å^2) and disfavor the higher +8 to +11 charge states which appear as more elongated ions (ca. 1100 to 1900 Å^2). At 46 °C (Figure 5b), near the T_m, the range of free energies (~18 kJ·mol^{-1}; ca. −3 to 15 kJ·mol^{-1}) is compressed such that the landscape is much flatter than at 26 °C. This compression results from both the destabilization of the 10 precursor structures as well as an overall stabilization of the 31 denatured states. Because of this balance in stability, at 46 °C each of the 41 structures is easily detected experimentally. This provides experimental insight about this system near the T_m. A two-state model assumes that at the T_m (where ΔG = 0 kJ·mol^{-1}), 50% of the native state population has unfolded to any number of denatured states such that the population of native and denatured structures is equal. Our data reveal that a few precursor states and product states are primarily responsible for this balance; however, many structures are populated. Finally, at 74 °C (Figure 5c), the precursor conformers have high, unfavorable free energies and the product conformers become the favored signals.

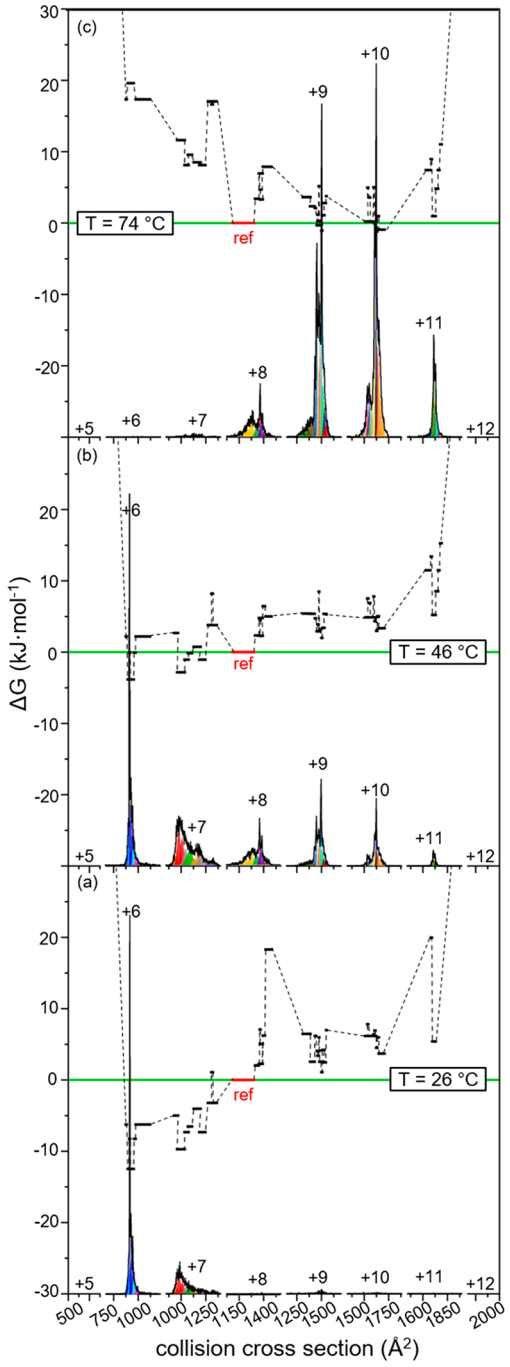

Figure 5. Free energy landscapes for the 41 wt conformational families on a cross section scale within each charge state at solution temperatures (a) 26, (b) 46, and (c) 74 °C. Families that have nearly zero abundance (ΔG > 20 kJ·mol^{-1}) are not included in this figure. Conformer P_1 is the thermodynamic reference state and is shown in red. The relative abundances of modeled collision cross section distributions for each charge state at the three temperatures are shown at the bottom of each free energy landscape.

Thermodynamic Analysis: Contributions of Enthalpy, Entropy, and the Key Role of Solvent in This System. As described above, the Gibbs−Helmholtz relationship (eq 5) describing ΔG as a function of temperature can be used to determine values of ΔH, ΔS, and ΔC_p for each solution state (see Figures S23−S25 for each Gibbs−Helmholtz fit). Figure 6a−c shows plots of ΔG (black), ΔH (blue), and $T\Delta S$ (red)

https://dx.doi.org/10.1021/jacs.0c05365
J. Am. Chem. Soc. 2020, 142, 17372−17383

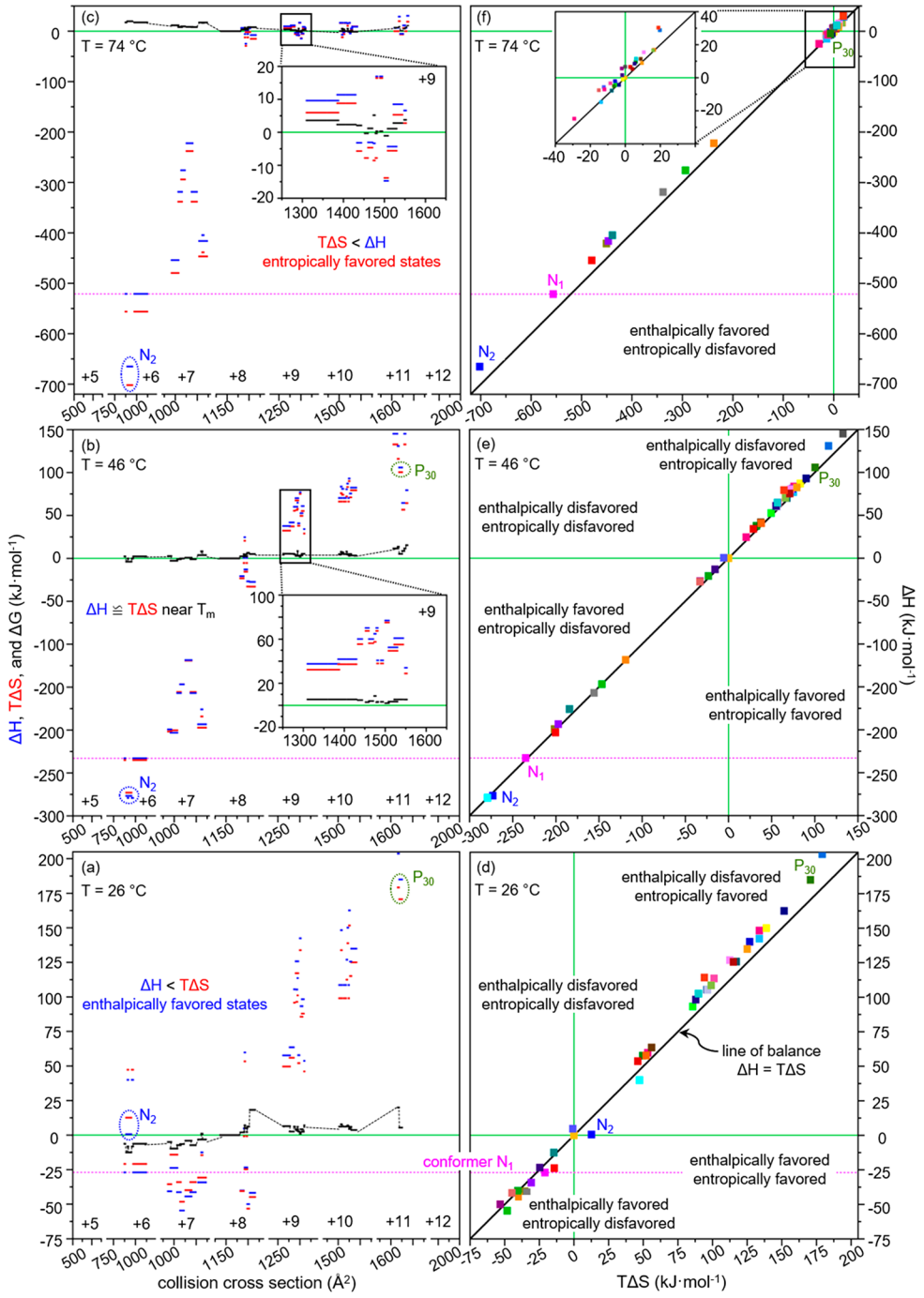

Figure 6. (a–c) Plots of ΔH in blue, $T\Delta S$ in red, and ΔG in black for each conformer family plotted on a cross section scale within each charge state at solution temperatures (a) 26, (b) 46, and (c) 74 °C. (d–f) Plots of entropy–enthalpy compensation (ΔH versus $T\Delta S$) for each state at the three temperatures where the color of each conformer family is denoted in Table S4. The line of balance indicates where $\Delta H = T\Delta S$ and $\Delta G = 0$.

on the same cross section scale for each charge state that was used in plotting ΔG at three representative temperatures. At first glance, one sees that at each temperature, the range of energies required to include all of the states that we have observed is far greater than was needed for the ΔG plot. On these scales, values of ΔG are so compressed (and near zero) that each free energy diagram appears relatively flat. This is because at equilibrium, ΔH and $T\Delta S$ must compensate for one another to establish a balance of thermodynamic factors associated with protein–protein, protein–solvent, and solvent–solvent interactions. Figure 6d–f illustrates this compensation by plotting values of ΔH versus $T\Delta S$ for each state. It is useful to consider how each quadrant of these plots is populated. Nearly all of the data points reside in the lower left or upper right quadrants because these are regions where $T\Delta S$ and ΔH compensate for one another. Tightly bound, energetically favorable states are disfavored by entropy (lower left quadrant) and dynamic conformations with favorable entropies are energetically unfavorable (upper right quadrant).

https://dx.doi.org/10.1021/jacs.0c05365
J. Am. Chem. Soc. 2020, 142, 17372–17383

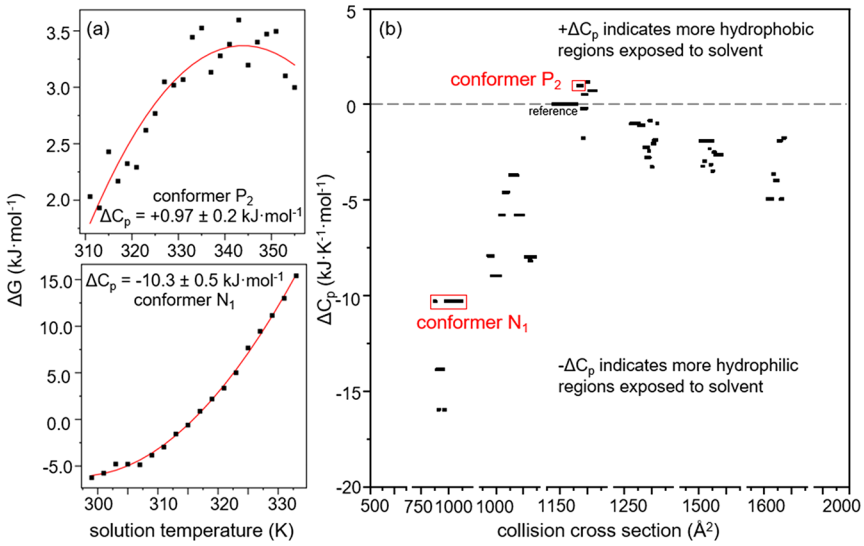

Figure 7. (a) Example Gibbs−Helmholtz fits for conformers P_2 and N_1. (b) ΔC_p as a function of charge state and collision cross section for each conformer family.

The large magnitudes of ΔH and $T\Delta S$ values and their respective temperature dependences are noteworthy. At low temperatures (26 °C, Figure 6a), the distribution of precursor states is highly favored enthalpically, with ΔH values ranging from ca. −50 to −25 kJ·mol^{-1} for the most abundant precursor species. Corresponding values of $T\Delta S$ for each of these species are extremely unfavorable. The distribution of native-like precursors is abundant because the magnitude of ΔH outweighs $T\Delta S$ in this region, as shown by Figure 6d in which many of the native-like precursor data points lie in the lower left quadrant and below the line of balance. At low temperatures, the low-abundance features that dominate at high temperatures (i.e., the product states) are energetically unfavorable, but more favorable values of $T\Delta S$ make such species observable.

At intermediate solution temperatures near the T_m (Figure 6b), the difference in $T\Delta S$ and ΔH values for each state diminishes and all structures fall along the line of balance shown in Figure 6e. At higher solution temperatures (Figure 6c), values of ΔH for the precursor states decrease substantially. Values of ΔH for the most intense precursor state (the conformer at 900 Å^2 observed for the +6 charge state) decrease from −30 kJ·mol^{-1} at 26 °C to −220 kJ·mol^{-1} and −520 kJ·mol^{-1} at 46 and 74 °C, respectively. In fact, the energies of all 41 structures become more favorable with respect to P_1 as the solution temperature is increased. In the case of the precursor states, this tremendous energetic stabilization (ΔH) is offset by an even larger unfavorable change in $T\Delta S$—disfavoring the precursor states. Nearly all of the product states are more favorable enthalpically and entropically at high temperatures. These states are ultimately favored entropically.

That an increase in temperature leads to an energetic stabilization of precursor states that decrease in abundance at high temperatures is somewhat paradoxical. At first glance one might expect precursor states to be enthalpically as well as entropically disfavored at high temperatures. To rationalize this, we begin by noting that this effect is also observed for product states. With this in mind, we imagined how changes in the solvent with increasing temperature might influence the stability of different structures. One physical property stands out. At low temperatures, water exists as a highly organized solvent with a dynamic and fluctuating hydrogen-bonded structure. This leads water to have an abnormally high dielectric constant (ε = 80 at 20 °C) making it exceptional as a solvent for shielding electrostatic interactions between solute molecules. As one expects, the entropy of water increases with increasing temperature—causing the network of hydrogen bonding interactions to become even more dynamic. In effect, the polarity of water decreases with increasing temperature and the less polar water has a substantially lower dielectric constant (ε = 58 at 90 °C).[66−68] Thus, the increase in entropy of the aqueous solvent has two effects—as expected, this more dynamic state of water disfavors the precursor states entropically, making them less accessible. However, the decrease in shielding would make all of the electrostatic interactions associated with tightly folded states (i.e., zwitterionic, charge−charge interactions, hydrogen bonding between polar groups, and van der Waals interactions) more favorable—leading to a decrease in the enthalpies for highly structured states such as the precursors.

Thermodynamic Analysis: Contributions of Heat Capacity. An additional thermodynamic parameter obtained by the Gibbs−Helmholtz analysis is ΔC_p which has energetic contributions from internal interactions within the protein and external interactions between the protein and solvent.[69−71] Ensemble protein unfolding is typically accompanied by a positive ΔC_p such that native conformers have small C_p values which elongate to form structures that have large positive C_p values.[22,46] In other words, a solution of folded protein will require less heat to raise its solution temperature than a solution of unfolded protein at the same concentration.[72] This is consistent with the behavior observed in Figure S22 for the overall melting transition obtained from the average charge state analysis for wt CI-2. The two-state transition can be fit over multiple temperature ranges. Figure S22a shows the Gibbs−Helmholtz fit from 297 to 345 K, and Figure S22b shows the data fit from 307 to 339 K. Both fits derive a positive change in heat capacity with temperature at either ΔC_p = 2.6 ± 1.1 kJ·mol^{-1}·K^{-1} (Figure S22a) or ΔC_p = 2.7 ± 1.2 kJ·mol^{-1}·K^{-1} (Figure S22b), both in good agreement with values obtained by DSC.[21]

https://dx.doi.org/10.1021/jacs.0c05365
J. Am. Chem. Soc. 2020, 142, 17372−17383

We have also used the Gibbs−Helmholtz analysis to calculate individual ΔC_p values for each of the 41 conformational families. In this way, we can analyze any changes in C_p for a single structure relative to reference P_1 as temperature is increased. Figure 7a shows example Gibbs−Helmholtz fits to temperature-dependent ΔG data for precursor state N_1 and product state P_2. The curvature in these data represents a nonzero value for ΔC_p[60] such that a concave-up curve as observed in the N_1 fit is attributed to a decrease in heat capacity with temperature and a concave-down curve signifies an increase in heat capacity with temperature as shown by the P_2 fit.

Figure 7b shows the ΔC_p of each conformational family with reference to P_1 on the same cross section scale as plots for ΔG, ΔH, and $T\Delta S$. The precursor states that comprise the +6 and +7 charge states show large negative values for ΔC_p such that there is an overall decrease in C_p with increasing temperature. The product states in the +8 distribution (centered around 1175 and 1300 Å^2) show a positive ΔC_p, while the rest of the product states have slightly negative ΔC_p values between −5 and 0 kJ·K^{-1}·mol^{-1}. Each static configuration exhibits a nonzero heat capacity which indicates that the interactions between the structures and the changing solvent properties at high temperatures likely drive the signs and magnitude of ΔC_p.

As described above, the aqueous solvent at high temperatures becomes less polar as its dielectric constant drops. This means that exposed hydrophobic residues will interact more favorably with the solvent at high temperatures thus driving the ΔC_p negative for hydrophobic (i.e., product) structures. Tightly folded states with buried hydrophobic residues interact less-favorably with the solvent at high temperatures, causing an increase in C_p for folded structures. However, the intramolecular interactions at high temperatures become extraordinarily favorable according to values of ΔH, a phenomenon that likely offsets the slight decrease in favorable protein−solvent interactions. Thus, the strong temperature dependence of ΔH and ΔS for folded structures (i.e., large decreases in ΔH and the subsequent compensation of ΔS) at high temperatures is likely a result of the large negative values of ΔC_p.

In previous studies, Fu and Freire[73] along with Velicelebi and Sturtevant[70] observed decreases in ΔC_p with increasing alcohol content. Similarly, the dielectric of the high-temperature aqueous environment in these studies resembles a 50:50 water:methanol mixture (ε = 61 at 25 °C),[74] further explaining why nearly all conformers exhibit a negative ΔC_p as the solvent becomes more nonpolar. A caveat to these interpretations is that one must consider the choice of reference state which also has (unmeasured) changing thermochemical properties with temperature. The ΔC_p values ultimately signify whether C_p for a given conformer is increasing or decreasing relative to the reference configuration, P_1. It may be the case that the reference structure is particularly hydrophobic which would drive ΔC_p for all other structures negative.

CONCLUSIONS

Anfinsen's thermodynamic hypothesis—that "the particular configuration that a protein assumes, under any specific set of conditions, is the one that is thermodynamically the most stable"—suggests that many configurations should be favored upon changing environmental factors.[1] However, rarely are these species observed experimentally. In this work, we took advantage of the exceptional sensitivity and dynamic range of vT-ESI-IMS-MS to examine the well-studied CI-2 system (and three nearly identical forms, each having a single amino acid substitution) at 30 solution temperatures (from 22 to 80 °C) with the aim of characterizing low-abundance "non-native" configurations. Consistent with this hypothesis, we presented an analysis and simple model of these data suggesting 41 distinct solution species that undergo structural transitions with unique temperature profiles. Ten of these appear to correspond to "native-like" precursor states. These are favored near room temperature and become unstable and less abundant as the solution temperature is increased beyond the melting temperature. From our model, we interpret 31 conformers that are favored at elevated temperatures as products of solution melting.

It is important to stress that our analysis depends on how the experimental charge states and IMS distributions are modeled. We believe that the approach presented above provides the most accurate representation of all four systems at all temperatures. An attractive feature of this model is that the peak positions and peak widths are fixed for all datasets. The only variable that changes in representing the datasets with this model is the abundance of different structures. That said, our model may overfit or underfit these data—suggesting more or fewer unique solution species than are actually present, respectively. It is also possible that as the resolving power of IMS techniques improve, we will find additional states that are obscured in our analysis. Regardless, the results provide a new experimental approach to the long-standing problem of measuring the complexity of structural transitions in proteins.

Within the model that is presented, it is interesting to consider the physical and chemical origins of these assignments. The temperature-dependent MS data, showing changes in the weighted average charge state distributions, provide information about the relative stabilities of each protein sequence as an overall melting temperature—in good agreement with DSC measurements and prior studies.[21,27] A clue about the many-state nature of this system was that individual charge states varied independently with temperature, suggesting that structural changes result in exposure of new basic residues reflecting different types of conformations from solution. Because of the exceptional sensitivity and dynamic range of these techniques it is possible to quantify many additional species and equilibria from solution. Within each charge state, collision cross section distributions for the wt and each mutant form show additional features that also change uniquely with solution temperature.

A Gibbs−Helmholtz analysis was used to derive thermodynamic properties (ΔG, ΔH, ΔS, and ΔC_p) for each state. As the temperature is increased, all configurations become more stable enthalpically; however, unfavorable changes in entropy compensate in a way that prohibits formation of the stable folded structures at high temperatures. We propose that the increase in enthalpic stabilities at high temperatures arises because of changes in the solvent; at high temperatures, water is less ordered and the dielectric constant drops. This decrease in the ability of water to shield electrostatic interactions leads to an increase in all short-range stabilizing interactions (i.e., zwitterionic, hydrogen, and van der Waals bonding) within the protein conformer. At all temperatures, enthalpy and entropy are closely balanced (i.e., $\Delta H \approx T\Delta S$). Above and below the T_m of each, this balance is harder to maintain, and slight offsets control the populations of native and denatured states.

Although these data provide an experimental measure of the properties (charge, shape, ΔG, ΔH, ΔS, and ΔC_p) of many

https://dx.doi.org/10.1021/jacs.0c05365
J. Am. Chem. Soc. 2020, 142, 17372−17383

conformations that exist during a structural transition, the issue of structural characterization of non-native states remains elusive. Advances in other types of spectroscopies[8,75,76] may complement these measurements to provide details about non-native configurations in solution. In the meantime, these data are useful as structural constraints. As noted by many, collision cross sections are a measure of the shapes of protein conformations in the gas phase.[4,23,24,34,38,39,41,45,53,77,78] Substantial progress in theory is making it possible to accurately model and calculate trial conformers for assignment of specific IMS peaks. Anhydrous structures may one day be computationally solvated to reveal their antecedent solution structures. The change in charge that is observed upon ionization under different solution conditions provides an additional constraint. Finally, the thermodynamic properties of these configurations should be testable by theory. Calculations of entropies and enthalpies for specific solution configurations will further restrict candidate structures; and, ΔC_p is known to be associated with differences in the solvent exposure of more or less polar side chains,[46] a property that offers substantial potential for characterizing structures as well as transitions between configurations.

■ ASSOCIATED CONTENT

Supporting Information

The Supporting Information is available free of charge at https://pubs.acs.org/doi/10.1021/jacs.0c05365.

Additional experimental and instrumentation details (mutant selection, sample preparation, converting drift times to cross sections, ESI considerations and vT-ESI source design, Gaussian modeling of IMS-MS distributions, choice of thermodynamic reference point, assumptions for Gibbs−Helmholtz analysis, uncertainties in MS and IMS measurements and derived thermochemical values); Figures S1−S25 and Tables S1−S8, depicting 4-m IMS-MS instrument, vT-ESI source, mass spectra at different solution temperatures and replicate MS analysis for all four sequences, CCS duplicate analysis for wt and K11A data, a comparison of extracted thermochemistry to literature values, the thermal behavior of the charge states, the reversible folding of CI-2, details of the Gaussian model presented, modeled temperature-dependent cross section data for the mutants, grouping analysis described for wt and mutants, the complete grouping analysis for all 41 conformational families, wt ΔG values at each temperature for each conformational family, and wt Gibbs−Helmholtz fits for each conformational family; and a list of supplementary references (PDF)

■ AUTHOR INFORMATION

Corresponding Author

David E. Clemmer − *Department of Chemistry, Indiana University, Bloomington, Indiana 47401, United States;* orcid.org/0000-0003-4039-1360; Email: clemmer@indiana.edu

Authors

Shannon A. Raab − *Department of Chemistry, Indiana University, Bloomington, Indiana 47401, United States*

Tarick J. El-Baba − *Department of Chemistry, Indiana University, Bloomington, Indiana 47401, United States*

Daniel W. Woodall − *Department of Chemistry, Indiana University, Bloomington, Indiana 47401, United States*

Wen Liu − *Department of Chemistry, Texas A&M University, College Station, Texas 77843, United States;* orcid.org/0000-0002-4804-2918

Yang Liu − *Department of Chemistry, Texas A&M University, College Station, Texas 77843, United States*

Zane Baird − *Baxter Healthcare Corporation, Bloomington, Indiana 47403, United States*

David A. Hales − *Department of Chemistry, Hendrix College, Conway, Arkansas 72032, United States*

Arthur Laganowsky − *Department of Chemistry, Texas A&M University, College Station, Texas 77843, United States;* orcid.org/0000-0001-5012-5547

David H. Russell − *Department of Chemistry, Texas A&M University, College Station, Texas 77843, United States;* orcid.org/0000-0003-0830-3914

Complete contact information is available at: https://pubs.acs.org/10.1021/jacs.0c05365

Notes

The authors declare no competing financial interest.

■ ACKNOWLEDGMENTS

This work is supported in part by funds from the National Institutes of Health, Grants 5R01GM121751-03 (D.E.C.), 5R01GM131100-02 (D.E.C.), and P41GM128577 (D.H.R.), the National Institute of General Medical Sciences, Grant DP2GM123486 (A.L.), the Robert and Marjorie Mann Graduate Research Fellowship from the Indiana University College of Arts and Sciences (S.A.R., D.W.W.), and the Dissertation Research Award from the Indiana University College of Arts and Sciences (T.J.E.).

■ REFERENCES

(1) Epstein, C. J.; Goldberger, R. F.; Anfinsen, C. B. The Genetic Control of Tertiary Protein Structure: Studies With Model Systems. *Cold Spring Harbor Symp. Quant. Biol.* **1963**, *28*, 439−449.

(2) Mirza, U. A.; Cohen, S. L.; Chait, B. T. Heat-induced conformational changes in proteins studied by electrospray ionization mass spectrometry. *Anal. Chem.* **1993**, *65*, 1−6.

(3) El-Baba, T. J.; Woodall, D. W.; Raab, S. A.; Fuller, D. R.; Laganowsky, A.; Russell, D. H.; Clemmer, D. E. Melting proteins: evidence for multiple stable structures upon thermal denaturation of native ubiquitin from ion mobility spectrometry-mass spectrometry measurements. *J. Am. Chem. Soc.* **2017**, *139*, 6306−6309.

(4) Wyttenbach, T.; Bowers, M. T. Structural stability from solution to the gas phase: native solution structure of ubiquitin survives analysis in a solvent-free ion mobility-mass spectrometry environment. *J. Phys. Chem. B* **2011**, *115*, 12266−12275.

(5) Shi, H.; Clemmer, D. E. Evidence for Two New Solution States of Ubiquitin by IMS-MS Analysis. *J. Phys. Chem. B* **2014**, *118*, 3498−3506.

(6) Anderson, D. E.; Becktel, W. J.; Dahlquist, F. W. pH-induced denaturation of proteins: a single salt bridge contributes 3−5 kcal/mol to the free energy of folding of T4 lysozyme. *Biochemistry* **1990**, *29*, 2403−2408.

(7) Vouret-Craviari, V.; Grall, D.; Chambard, J. C.; Rasmussen, U. B.; Pouyssegur, J.; Van Obberghen-Schilling, E. Post-translational and activation-dependent modifications of the G protein-coupled thrombin receptor. *J. Biol. Chem.* **1995**, *270*, 8367−8372.

(8) Houde, D.; Peng, Y.; Berkowitz, S. A.; Engen, J. R. Post-translational modifications differentially affect IgG1 conformation and receptor binding. *Mol. Cell. Proteomics* **2010**, *9*, 1716−1728.

(9) Walsh, G.; Jefferis, R. Post-translational modifications in the context of therapeutic proteins. *Nat. Biotechnol.* **2006**, *24*, 1241.
(10) Xie, Y.; Zhang, J.; Yin, S.; Loo, J. A. Top-down ESI-ECD-FT-ICR mass spectrometry localizes noncovalent protein-ligand binding sites. *J. Am. Chem. Soc.* **2006**, *128*, 14432−14433.
(11) Woodall, D. W.; El-Baba, T. J.; Fuller, D. R.; Liu, W.; Brown, C. J.; Laganowsky, A.; Russell, D. H.; Clemmer, D. E. Variable-Temperature ESI-IMS-MS Analysis of Myohemerythrin Reveals Ligand Losses, Unfolding, and a Non-Native Disulfide Bond. *Anal. Chem.* **2019**, *91*, 6808−6814.
(12) Brockwell, D. J.; Radford, S. E. Intermediates: ubiquitous species on folding energy landscapes? *Curr. Opin. Struct. Biol.* **2007**, *17*, 30−37.
(13) Daggett, V.; Fersht, A. R. The present view of the mechanism of protein folding. *Nat. Rev. Mol. Cell Biol.* **2003**, *4*, 497−502.
(14) Lazaridis, T.; Karplus, M. New view of protein folding reconciled with the old through multiple unfolding simulations. *Science* **1997**, *278*, 1928−1931.
(15) Karplus, M.; McCammon, J. A. Molecular dynamics simulations of biomolecules. *Nat. Struct. Biol.* **2002**, *9*, 646−652.
(16) Dill, K. A.; Chan, H. S. From Levinthal to pathways to funnels. *Nat. Struct. Mol. Biol.* **1997**, *4*, 10−19.
(17) Karplus, M.; Šali, A. Theoretical studies of protein folding and unfolding. *Curr. Opin. Struct. Biol.* **1995**, *5*, 58−73.
(18) Kazmirski, S. L.; Wong, K. B.; Freund, S. M.; Tan, Y. J.; Fersht, A. R.; Daggett, V. Protein folding from a highly disordered denatured state: the folding pathway of chymotrypsin inhibitor 2 at atomic resolution. *Proc. Natl. Acad. Sci. U. S. A.* **2001**, *98*, 4349−4354.
(19) Lumry, R.; Eyring, H. Conformation changes of proteins. *J. Phys. Chem.* **1954**, *58*, 110−120.
(20) Bohrer, B. C.; Merenbloom, S. I.; Koeniger, S. L.; Hilderbrand, A. E.; Clemmer, D. E. Biomolecule analysis by ion mobility spectrometry. *Annu. Rev. Anal. Chem.* **2008**, *1*, 293−327.
(21) Jackson, S. E.; Fersht, A. R. Folding of chymotrypsin inhibitor 2. 1. Evidence for a two-state transition. *Biochemistry* **1991**, *30*, 10428−10435.
(22) Fersht, A. *Structure and mechanism in protein science: a guide to enzyme catalysis and protein folding*; W. H. Freeman and Co.: New York, 1999.
(23) Pierson, N. A.; Chen, L.; Valentine, S. J.; Russell, D. H.; Clemmer, D. E. Number of solution states of bradykinin from ion mobility and mass spectrometry measurements. *J. Am. Chem. Soc.* **2011**, *133*, 13810−13813.
(24) Silveira, J. A.; Fort, K. L.; Kim, D.; Servage, K. A.; Pierson, N. A.; Clemmer, D. E.; Russell, D. H. From solution to the gas phase: stepwise dehydration and kinetic trapping of Substance P reveals the origin of peptide conformations. *J. Am. Chem. Soc.* **2013**, *135*, 19147−19153.
(25) McPhalen, C. A.; James, M. N. G. Crystal and molecular structure of the serine proteinase inhibitor CI-2 from barley seeds. *Biochemistry* **1987**, *26*, 261−269.
(26) Ludvigsen, S.; Shen, H.; Kjær, M.; Madsen, J. C.; Poulsen, F. M. Refinement of the three-dimensional solution structure of barley serine proteinase inhibitor 2 and comparison with the structures in crystals. *J. Mol. Biol.* **1991**, *222*, 621−635.
(27) Itzhaki, L. S.; Otzen, D. E.; Fersht, A. R. The structure of the transition state for folding of chymotrypsin inhibitor 2 analysed by protein engineering methods: evidence for a nucleation-condensation mechanism for protein folding. *J. Mol. Biol.* **1995**, *254*, 260−288.
(28) Jackson, S. E.; Moracci, M.; Elmasry, N.; Johnson, C. M.; Fersht, A. R. Effect of cavity-creating mutations in the hydrophobic core of chymotrypsin inhibitor 2. *Biochemistry* **1993**, *32*, 11259−11269.
(29) Shi, L.; Holliday, A. E.; Glover, M. S.; Ewing, M. A.; Russell, D. H.; Clemmer, D. E. Ion Mobility-Mass Spectrometry Reveals the Energetics of Intermediates that Guide Polyproline Folding. *J. Am. Soc. Mass Spectrom.* **2016**, *27*, 22−30.
(30) Conant, C. R.; Fuller, D. R.; El-Baba, T. J.; Zhang, Z.; Russell, D. H.; Clemmer, D. E. Substance P in Solution: Trans-to-Cis Configurational Changes of Penultimate Prolines Initiate Non-enzymatic Peptide Bond Cleavages. *J. Am. Soc. Mass Spectrom.* **2019**, *30*, 919−931.
(31) Fuller, D. R.; Conant, C. R.; El-Baba, T. J.; Brown, C. J.; Woodall, D. W.; Russell, D. H.; Clemmer, D. E. Conformationally regulated peptide bond cleavage in bradykinin. *J. Am. Chem. Soc.* **2018**, *140*, 9357−9360.
(32) Loo, J. A.; Loo, R. R. O.; Udseth, H. R.; Edmonds, C. G.; Smith, R. D. Solvent-induced conformational changes of polypeptides probed by electrospray-ionization mass spectrometry. *Rapid Commun. Mass Spectrom.* **1991**, *5* (3), 101−105.
(33) Jarrold, M. F.; Constant, V. A. Silicon cluster ions: Evidence for a structural transition. *Phys. Rev. Lett.* **1991**, *67*, 2994−2997.
(34) Von Helden, G.; Hsu, M. T.; Kemper, P. R.; Bowers, M. T. Structures of carbon cluster ions from 3 to 60 atoms: Linears to rings to fullerenes. *J. Chem. Phys.* **1991**, *95*, 3835−3837.
(35) Shvartsburg, A. A. Ultrahigh-resolution differential ion mobility separations of conformers for proteins above 10 kDa: onset of dipole alignment? *Anal. Chem.* **2014**, *86*, 10608−10615.
(36) Wagner, N.; Clemmer, D. E.; Russell, D. H. ESI-IM-MS and Collision-Induced Unfolding Provide Insight into the Linkage Dependent Interfacial Interactions of Covalently Linked Diubiquitin. *Anal. Chem.* **2017**, *89*, 10094−10103.
(37) Koeniger, S. L.; Clemmer, D. E. Resolution and Structural Transitions of Elongated States of Ubiquitin. *J. Am. Soc. Mass Spectrom.* **2007**, *18*, 322−331.
(38) Clemmer, D. E.; Jarrold, M. F. Ion mobility measurements and their applications to clusters and biomolecules. *J. Mass Spectrom.* **1997**, *32*, 577−592.
(39) Clemmer, D. E.; Hudgins, R. R.; Jarrold, M. F. Naked protein conformations: cytochrome c in the gas phase. *J. Am. Chem. Soc.* **1995**, *117*, 10141−10142.
(40) Wyttenbach, T.; Kemper, P. R.; Bowers, M. T. Design of a new electrospray ion mobility mass spectrometer. *Int. J. Mass Spectrom.* **2001**, *212*, 13−23.
(41) Bleiholder, C.; Bowers, M. T. The Solution Assembly of Biological Molecules using Ion Mobility Methods: From Amino Acids to Amyloid β-Protein. *Annu. Rev. Anal. Chem.* **2017**, *10*, 365−386.
(42) Zhong, Y.; Hyung, S. J.; Ruotolo, B. T. Ion mobility-mass spectrometry for structural proteomics. *Expert Rev. Proteomics* **2012**, *9*, 47−58.
(43) Uetrecht, C.; Rose, R. J.; van Duijn, E.; Lorenzen, K.; Heck, A. J. Ion mobility mass spectrometry of proteins and protein assemblies. *Chem. Soc. Rev.* **2010**, *39*, 1633−1655.
(44) Anderson, S. E.; Mitchell, C.; Haddad, T. S.; Vij, A.; Schwab, J. J.; Bowers, M. T. Structural characterization of POSS siloxane dimer and trimer. *Chem. Mater.* **2006**, *18*, 1490−1497.
(45) Bush, M. F.; Hall, Z.; Giles, K.; Hoyes, J.; Robinson, C. V.; Ruotolo, B. T. Collision cross sections of proteins and their complexes: a calibration framework and database for gas-phase structural biology. *Anal. Chem.* **2010**, *82*, 9557−9565.
(46) Prabhu, N. V.; Sharp, K. A. Heat capacity in proteins. *Annu. Rev. Phys. Chem.* **2005**, *56*, 521−548.
(47) Koeniger, S. L.; Merenbloom, S. I.; Clemmer, D. E. Evidence for many resolvable structures within conformation types of electrosprayed ubiquitin ions. *J. Phys. Chem. B* **2006**, *110*, 7017−7021.
(48) Merenbloom, S. I.; Koeniger, S. L.; Valentine, S. J.; Plasencia, M. D.; Clemmer, D. E. IMS-IMS and IMS-IMS-IMS/MS for separating peptide and protein fragment ions. *Anal. Chem.* **2006**, *78*, 2802−2809.
(49) Hoaglund, C. S.; Valentine, S. J.; Sporleder, C. R.; Reilly, J. P.; Clemmer, D. E. Three-dientional ion mobility/TOFMS analysis of electrosprayed biomolecules. *Anal. Chem.* **1998**, *70*, 2236−2242.
(50) Koeniger, S. L.; Merenbloom, S. I.; Valentine, S. J.; Jarrold, M. F.; Udseth, H.; Smith, R. D.; Clemmer, D. E. An IMS-MS Analogue of MS-MS. *Anal. Chem.* **2006**, *78*, 4161−4174.
(51) Mason, E. A.; McDaniel, E. W. *Transport properties of ions in gases*; John Wiley & Sons: Hoboken, NJ, 1988.

https://dx.doi.org/10.1021/jacs.0c05365
J. Am. Chem. Soc. 2020, 142, 17372−17383

(52) Hoaglund-Hyzer, C. S.; Counterman, A. E.; Clemmer, D. E. Anhydrous protein ions. *Chem. Rev.* **1999**, *99*, 3037−3079.
(53) Shvartsburg, A. A.; Jarrold, M. F. An exact hard spheres scattering model for the mobilities of polyatomic ions. *Chem. Phys. Lett.* **1996**, *261*, 86−91.
(54) Schaffer, S. A.; Tang, K.; Anderson, G. A.; Prior, D. C.; Udseth, H. R.; Smith, R. D. A novel ion funnel for focusing ions at elevated pressure using electrospray ionization mass spectrometry. *Rapid Commun. Mass Spectrom.* **1997**, *11*, 1813−1817.
(55) Shaffer, S. A.; Prior, D. C.; Anderson, G. A.; Udseth, H. R.; Smith, R. D. An ion funnel interface for improved ion focusing and sensitivity using electrospray ionization mass spectrometry. *Anal. Chem.* **1998**, *70*, 4111−4119.
(56) Cong, X.; Liu, Y.; Liu, W.; Liang, X.; Russell, D. H.; Laganowsky, A. Determining membrane protein-lipid binding thermodynamics using native mass spectrometry. *J. Am. Chem. Soc.* **2016**, *138*, 4346−4349.
(57) Wang, G.; Abzalimov, R. R.; Kaltashov, I. A. Direct monitoring of heat-stressed biopolymers with temperature-controlled electrospray ionization mass spectrometry. *Anal. Chem.* **2011**, *83*, 2870−2876.
(58) Sterling, H. J.; Williams, E. R. Origin of supercharging in electrospray ionization of noncovalent complexes from aqueous solution. *J. Am. Soc. Mass Spectrom.* **2009**, *20*, 1933−1943.
(59) Benesch, J. L. P.; Sobott, F.; Robinson, C. V. Thermal dissociation of multimeric protein complexes by using nano-electrospray mass spectrometry. *Anal. Chem.* **2003**, *75*, 2208−2214.
(60) LiCata, V. J.; Liu, C.-C. Analysis of free energy versus temperature curves in protein folding and macromolecular interactions. *Methods Enzymol.* **2011**, *488*, 219−238.
(61) Chowdhury, S. K.; Katta, V.; Chait, B. T. Probing conformational changes in proteins by mass spectrometry. *J. Am. Chem. Soc.* **1990**, *112*, 9012−9013.
(62) Šamalikova, M.; Matečko, I.; Müller, N.; Grandori, R. Interpreting conformational effects in protein nano-ESI-MS spectra. *Anal. Bioanal. Chem.* **2004**, *378*, 1112−1123.
(63) Wagner, D. S.; Anderegg, R. J. Conformation of cytochrome c studied by deuterium exchange-electrospray ionization mass spectrometry. *Anal. Chem.* **1994**, *66*, 706−711.
(64) Dobo, A.; Kaltashov, I. A. Detection of multiple protein conformational ensembles in solution via deconvolution of charge-state distributions in ESI MS. *Anal. Chem.* **2001**, *73*, 4763−4773.
(65) Valentine, S. J.; Counterman, A. E.; Clemmer, D. E. A database of 660 peptide ion cross sections: use of intrinsic size parameters for bona fide predictions of cross sections. *J. Am. Soc. Mass Spectrom.* **1999**, *10*, 1188−1211.
(66) Owen, B. B.; Miller, R. C.; Milner, C. E.; Cogan, H. L. The Dielectric Constant of Water As a Function of Temperature and Pressure. *J. Phys. Chem.* **1961**, *65*, 2065−2070.
(67) Akerlof, G. C.; Oshry, H. I. The dielectric constant of water at high temperatures and in equilibrium with its vapor. *J. Am. Chem. Soc.* **1950**, *72*, 2844−2847.
(68) Malmberg, C. G.; Maryott, A. A. Dielectric constant of water from 0° to 100° C. *J. Res. Natl. Bur. Stand.* **1956**, *56*, 1−8.
(69) Madan, B.; Sharp, K. Heat capacity changes accompanying hydrophobic and ionic solvation: a Monte Carlo and random network model study. *J. Phys. Chem.* **1996**, *100*, 7713−7721.
(70) Velicelebi, G.; Sturtevant, J. M. Thermodynamics of the denaturation of lysozyme in alcohol-water mixtures. *Biochemistry* **1979**, *18*, 1180−1186.
(71) Privalov, P. L.; Makhatadze, G. I. Heat capacity of proteins: II. Partial molar heat capacity of the unfolded polypeptide chain of proteins: protein unfolding effects. *J. Mol. Biol.* **1990**, *213*, 385−391.
(72) Robertson, A. D.; Murphy, K. P. Protein structure and the energetics of protein stability. *Chem. Rev.* **1997**, *97*, 1251−1268.
(73) Fu, L.; Freire, E. On the origin of the enthalpy and entropy convergence temperatures in protein folding. *Proc. Natl. Acad. Sci. U. S. A.* **1992**, *89*, 9335−9338.
(74) Albright, P. S.; Gosting, L. J. Dielectric constants of the methanol-water system from 5 to 55°. *J. Am. Chem. Soc.* **1946**, *68*, 1061−1063.
(75) Rizzo, T. R.; Stearns, J. A.; Boyarkin, O. V. Spectroscopic studies of cold, gas-phase biomolecular ions. *Int. Rev. Phys. Chem.* **2009**, *28*, 481−515.
(76) Oomens, J.; Sartakov, B. G.; Meijer, G.; von Helden, G. Gas-phase infrared multiple photon dissociation spectroscopy of mass-selected molecular ions. *Int. J. Mass Spectrom.* **2006**, *254*, 1−19.
(77) Smith, D. P.; Knapman, T. W.; Campuzano, I.; Malham, R. W.; Berryman, J. T.; Radford, S. E.; Ashcroft, A. E. Deciphering drift time measurements from travelling wave ion mobility spectrometry-mass spectrometry studies. *Eur. J. Mass Spectrom.* **2009**, *15*, 113−130.
(78) Clemmer, D. E.; Russell, D. H.; Williams, E. R. Characterizing the Conformationome: Toward a Structural Understanding of the Proteome. *Acc. Chem. Res.* **2017**, *50* (3), 556−560.

https://dx.doi.org/10.1021/jacs.0c05365
J. Am. Chem. Soc. 2020, 142, 17372−17383